AQUAMARINE, MAXIXE-TYPE BERYL, AND HYDROTHERMAL SYNTHETIC BLUE BERYL: ANALYSIS AND IDENTIFICATION

Ilaria Adamo, Alessandro Pavese, Loredana Prosperi, Valeria Diella,
David Ajò, G. Diego Gatta, and Christopher P. Smith

Aquamarine, Maxixe-type (irradiated) beryl, and two types of hydrothermally grown synthetic blue beryl currently available in the marketplace were investigated by classical gemological methods, chemical analysis, and UV-Vis-NIR and mid-IR spectroscopy. These materials may be conclusively identified by a combination of these techniques. The Maxixe-type beryl (like natural-color Maxixe beryls) is distinguishable by its unusual dichroism, green UV fluorescence (when present), Fe-free chemical composition, and distinctive UV-Vis-NIR spectrum. The hydrothermal synthetic blue beryls can be discriminated from their natural counterparts on the basis of microscopic features, chemical composition, and visible and infrared spectroscopic features.

Aquamarine has been one of the most popular gem materials for centuries, prized for its beauty and rarity. The color of aquamarine ranges from the familiar light blue to blue-green hues, to a rarer highly saturated dark blue (e.g., Rohtert et al., 2003; Laurs, 2005). However, a deep blue color is more typically associated with the color variety known as Maxixe beryl, discovered for the first time in Brazil in 1917 (Roebling and Tromnau, 1935; Schlossmacher and Klang, 1935), which typically fades on exposure to light. Similar beryl specimens appeared in the market around 1973, but such material was artificially irradiated and was thus called *Maxixe-type* beryl (Nassau et al., 1976).

Synthetic blue beryl has been produced by hydrothermal growth techniques since the late 1980s (Koivula and Kammerling, 1988, 1991; Nassau, 1990, 1997). Tairus, a Thai/Russian joint venture, produces synthetic blue beryl in Russia and markets it out of Bangkok (Smirnov et al., 1999). A new hydrothermal synthetic blue beryl was unveiled by Malossi Gemme Create, Milan, Italy, during the 2006 Las Vegas JCK Show (A. Malossi, pers. comm., 2007).

This article presents a full characterization of a suite of aquamarines and other blue beryls of different origins by classic gemological and contemporary analytical techniques, in order to determine those features that may be diagnostic for their identification.

MATERIALS AND METHODS

We examined a total of 25 natural, treated, and synthetic blue beryl specimens (see, e.g., figure 1): four faceted Brazilian aquamarines (0.18 to 1.54 ct); one faceted and one rough aquamarine from Nigeria (1.81 and 54.02 ct, respectively); three faceted (0.08–0.13 ct) and two rough (7.30 and 8.20 ct) aquamarines (marketed as "True Blue" beryl) from the Yukon Territory, Canada; one faceted Maxixe-type (irradiated) blue beryl (1.77 ct); three faceted Tairus hydrothermal synthetic blue beryls (2.03–3.50 ct);

See end of article for About the Authors and Acknowledgments.
GEMS & GEMOLOGY, Vol. 44, No. 3, pp. 214–226.

Figure 1. This study examined three varieties of blue beryl: aquamarine, Maxixe-type (irradiated) blue beryl, and hydrothermally grown synthetic blue beryl. Shown here are some of those samples: two aquamarines from Brazil (far left, 1.54 and 1.33 ct), one from Nigeria (bottom, 1.81 ct), one Maxixe-type beryl (center, 1.77 ct), two Tairus synthetics (top center, 2.03 ct and center right, 3.50 ct), and one Malossi synthetic (top right, 2.92 ct). Composite photo by Fred Kahn and Sun Joo Chung.

and eight faceted (2.70–5.12 ct) and two unfashioned (61.05 and 64.85 ct) Malossi hydrothermal synthetic blue beryls.

All the faceted samples were examined by standard gemological methods to determine their optical properties (refractive indices, birefringence, and pleochroism), specific gravity, UV fluorescence, and microscopic features.

Quantitative chemical analyses were performed on eight faceted samples (three aquamarines from Canada, one Maxixe-type beryl, and one Tairus and three Malossi synthetic blue beryls) using a JEOL JXA-8200 electron microprobe in wavelength-dispersive mode. The following elements were measured: Na, Mg, Al, Si, Cl, K, Ca, Ti, V, Cr, Mn, Fe, Cu, Rb, and Cs. The raw data were processed for matrix effects using a conventional ZAF routine from the JEOL series of programs.

Unpolarized spectroscopic measurements over the near-infrared (9000–4000 cm^{-1}) and mid-infrared (4000–400 cm^{-1}) ranges were carried out on all but the Nigerian samples using a Nicolet Nexus Fourier-transform infrared (FTIR) spectrometer equipped with a diffuse reflectance accessory (DRIFT) and operating with a resolution of 4 cm^{-1}.

Mid-IR spectra were also collected in transmission mode using KBr pellets (2 mg sample mixed with 200 mg KBr), confining the related sampling to portions of two unfashioned specimens (one Canadian aquamarine and one Malossi synthetic beryl).

Polarized ultraviolet-visible–near infrared (UV-Vis-NIR) spectroscopic measurements covering the 250–3300 nm range were performed with a Perkin Elmer Lambda 950 spectrometer using a calcite polarizer (1 nm scan interval) on all samples except the Canadian and Nigerian aquamarines.

RESULTS

Visual Appearance. Natural aquamarine typically ranges from greenish blue to (a purer) blue of low-to-moderate saturation with a light to medium-dark tone. The natural samples in this study varied in hue, tone, and saturation (again, see figure 1). The Canadian samples were darker and more saturated than either the Brazilian or Nigerian samples. The color of our Maxixe-type beryl was significantly more intense than that typically associated with aquamarine and had a slightly violet modifier. The Tairus and Malossi synthetic blue beryls were also significantly more saturated and much darker in tone than most aquamarine. The Malossi samples also had a distinct violet component.

Standard Gemological Properties. The standard gemological properties of the samples included in this study are summarized in table 1.

All the samples, with the exception of the Maxixe-type beryl, exhibited their stronger pleochroic color perpendicular to the c-axis (e-ray). As noted by

Figure 2. Multi-phase fluid inclusions are a common feature in natural aquamarine. Photomicrograph by C. P. Smith; magnified 65×.

Figure 3. The fine, parallel growth channels in this Maxixe-type beryl indicate the natural origin of the host. Photomicrograph by Giulio Chiodi; magnified 50×.

previous researchers, the stronger pleochroic color for Maxixe-type beryl is observed parallel to the c-axis (o-ray). The Maxixe-type beryl was also the only sample that was not inert to both long- and short-wave UV radiation.

Microscopy. The natural aquamarines and Maxixe-type beryl in this study had a wide variety of internal features indicative of their natural origin: single- and multi-phase fluid inclusions (figure 2), various patterns of healed fractures, crystalline inclusions, and growth tubes (figure 3), as

TABLE 1. Gemological properties of the natural and synthetic blue beryls investigated in this study.

Property	Natural				Synthetic	
	Aquamarine			Maxixe-type (irradiated)	Malossi	Tairus
	Brazil	Nigeria	Canada			
Color	Medium blue	Medium greenish blue	Dark grayish blue	Dark slightly violetish blue	Dark violetish blue	Dark grayish blue
Diaphaneity	Transparent	Transparent	Semitransparent to translucent	Transparent	Transparent	Transparent
Refractive indices	n_o = 1.586–1.590 n_e = 1.580–1.582	n_o = 1.586 n_e = 1.578	n_o = 1.601 n_e = 1.592–1.593	n_o = 1.588 n_e = 1.580	n_o = 1.590 n_e = 1.582	n_o = 1.586 n_e = 1.580
Birefringence	0.006–0.008	0.008	0.008–0.009	0.008	0.008	0.006
Specific gravity	2.76	2.67	2.80–2.87	2.75	2.75–2.77	2.71
Pleochroism[a]						
o-ray	Pale greenish blue	Pale greenish blue	Pale greenish blue	Dark blue	Pale blue	Pale greenish blue
e-ray	Medium blue	Medium blue	Dark blue	Colorless	Dark violetish blue	Dark blue
UV fluorescence						
Long-wave	Inert	Inert	Inert	Mod. deep green[b]	Inert	Inert
Short-wave	Inert	Inert	Inert	Mod. yellowish green	Inert	Inert
Internal features	Crystals, two-phase and liquid inclusions, "fingerprints," growth tubes, growth lines, fractures	Crystals, multi-phase inclusions, growth tubes, fractures	Crystals, multi-phase inclusions, "fingerprints," growth tubes, growth lines, fractures, evidence of clarity enhancement	Growth tubes, two-phase and liquid inclusions	Irregular growth structures, "fingerprints," fractures	Irregular growth structures, pinpoints, "fingerprints," fractures, seed plates

[a] *All samples were uniaxial negative, and they showed strong dichroism.*
[b] *Mod. = moderate.*

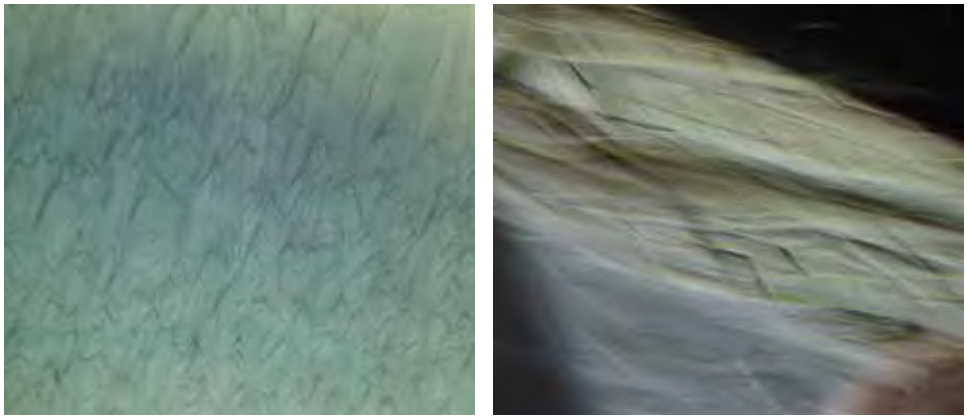

Figure 4. This Malossi hydrothermal synthetic blue beryl exhibits irregular growth features with a step-like shape that provide evidence of the sample's synthetic origin. Photomicrographs by Giulio Chiodi (left, in immersion, magnified 40×) and I. Adamo (right, magnified 35×).

well as straight and angular internal growth structures. Unhealed fractures were also observed in many of the aquamarine samples. However, the Canadian samples also revealed a blue and yellow "flash effect," as is commonly observed in gems that have been clarity enhanced (refer to the "Discussion" of the mid-infrared spectroscopy results below).

The Tairus and Malossi synthetic beryls also revealed several diagnostic internal features. Most notably, these consisted of distinctive irregular internal growth structures (figures 4 and 5). Present in samples from both sources, but more common in those from Tairus, were healed-fracture "fingerprints" (figure 6), as well as open fractures. In addition, all the Tairus synthetic samples contained groups of black pinpoint inclusions (figure 7), with remnants of the seed plates (in two out of the three Tairus samples; e.g., figure 8) that are indicative of the artificial growth process. We did not observe any of these black inclusions or seed-plate remnants in our Malossi synthetic samples.

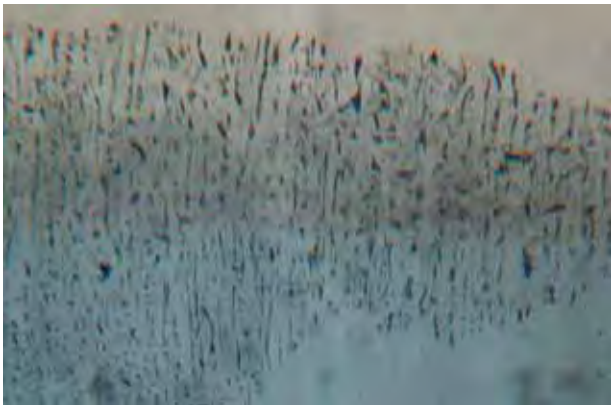

Figure 6. "Fingerprints" (healed fractures) such as this one in a Tairus sample were seen in both types of synthetics. Photomicrograph by Giulio Chiodi, in immersion; magnified 40×.

Figure 5. The Tairus hydrothermal synthetic samples also showed widespread irregular growth structures that demonstrate they are synthetic. Photomicrographs by I. Adamo (left, magnified 20×) and C. P. Smith (right, magnified 32×).

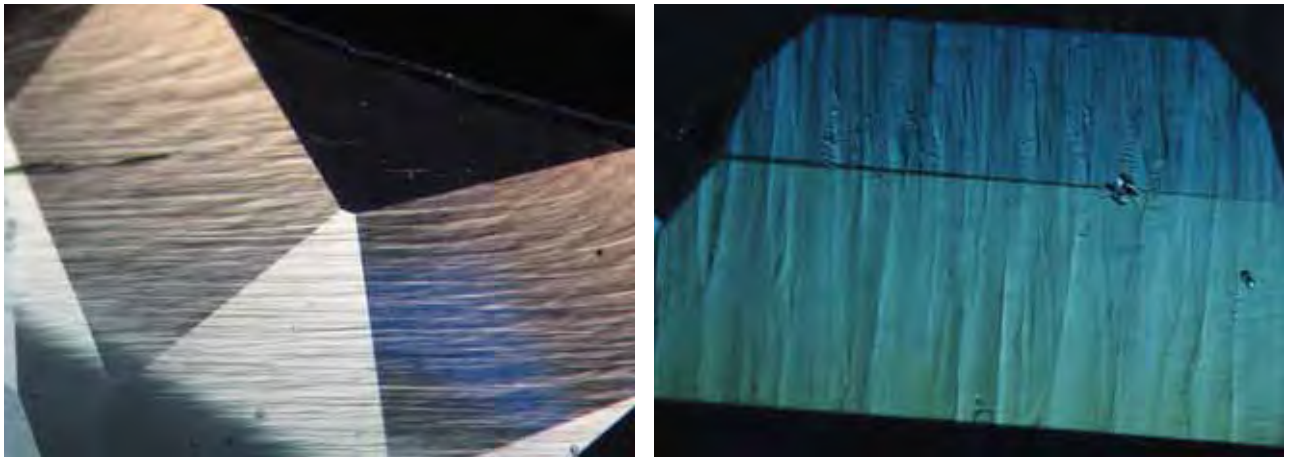

Figure 7. The Tairus synthetic beryls also contained numerous small, irregular black pinpoint inclusions. Photomicrographs by C. P. Smith (left, magnified 32×) and Giulio Chiodi (right, in immersion; magnified 50×).

Chemical Composition. The chemical compositions of three Canadian aquamarines, one Maxixe-type beryl, and one Tairus and three Malossi hydrothermally grown synthetic blue beryls are presented in table 2 and plotted in figure 9. The low totals can be ascribed to the presence of water in both natural and hydrothermal synthetic beryls (e.g., Wood and Nassau, 1968; Deer et al., 1986). Totals can also be affected by variable amounts of lithium, which—like H_2O—is undetectable by electron microprobe.

TABLE 2. Average electron-microprobe analyses for the natural and synthetic blue beryls investigated in this study.[a]

Chemical composition	Natural				Synthetic			
	Canada			Maxixe-type (irradiated)	Malossi			Tairus
Sample	1	2	3		A	B	C	
No. analyses	5	4	5	8	10	4	4	8
Oxides (wt.%)								
SiO_2	62.60	63.11	62.68	65.44	64.22	64.06	63.80	64.56
Al_2O_3	11.75	11.63	11.58	17.70	16.75	16.56	16.52	16.48
FeO[b]	5.04	5.03	4.96	bdl	1.96	1.95	2.50	2.75
MnO	bdl	bdl	bdl	bdl	0.15	0.13	0.10	bdl
K_2O	bdl	bdl	bdl	0.06	bdl	bdl	bdl	bdl
Na_2O	2.24	2.40	2.24	0.47	0.07	0.12	0.13	bdl
MgO	1.76	1.80	1.69	bdl	0.12	0.21	0.22	bdl
Cs_2O	bdl	bdl	bdl	0.70	bdl	bdl	bdl	bdl
CuO	bdl	bdl	bdl	bdl	2.95	1.69	1.57	bdl
BeO[c]	12.91	12.99	12.88	13.56	12.40	12.76	12.79	13.37
Total	96.30	96.96	96.03	97.93	98.62	97.48	97.63	97.16
Ions calculated on 18 oxygens								
Si	6.058	6.068	6.079	6.028	6.018	6.021	6.002	6.032
Al	1.340	1.318	1.323	1.922	1.850	1.835	1.831	1.814
Fe	0.408	0.404	0.402	bdl	0.154	0.153	0.197	0.215
Mn	bdl	bdl	bdl	bdl	0.012	0.011	0.008	bdl
K	bdl	bdl	bdl	0.007	bdl	bdl	bdl	bdl
Na	0.420	0.448	0.422	0.084	0.013	0.022	0.023	bdl
Mg	0.254	0.258	0.244	bdl	0.017	0.030	0.030	bdl
Cs	bdl	bdl	bdl	0.028	bdl	bdl	bdl	bdl
Cu	bdl	bdl	bdl	bdl	0.209	0.120	0.112	bdl

[a] *Instrument operating conditions: accelerating voltage = 15 kV, beam current = 15 nA, count time = 20 seconds on peaks and 5 seconds on background. Standards: natural wollastonite (for Si, Ca), anorthite (for Al), fayalite (for Fe), olivine (for Mg), rhodonite (for Mn), omphacite (for Na), ilmenite (for Ti), K-feldspar (for K), pollucite (for Cs), and sodalite (for Cl); pure V, Rb, Cr, and Cu for those elements. Abbreviation: bdl = below detection limit (in wt.%): 0.05 FeO, 0.08 CuO, 0.04 MnO, 0.04 K_2O, 0.05 Na_2O, 0.05 MgO, 0.04 Cs_2O. Chlorine, calcium, titanium, vanadium, chromium, and rubidium were below the detection limit (0.05 wt.%) in all analyses.*

[b] *Total iron is calculated as FeO.*

[c] *Calculated assuming (Be+Cu)/Si=0.5.*

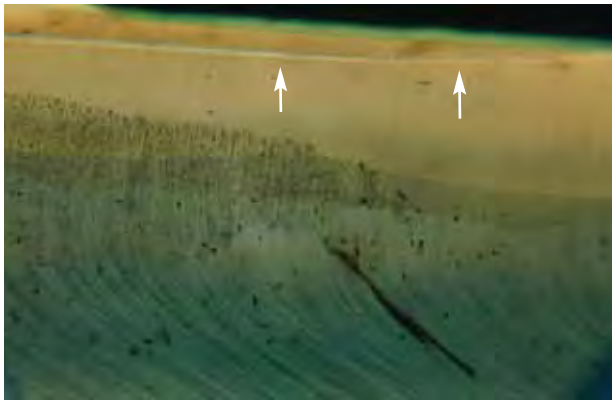

Figure 8. Two of the Tairus synthetic beryls had remnants of the seed plate (see arrows). When present, this provides proof of synthetic origin. Note the widespread irregular growth structures, pinpoint inclusions, and "fingerprints." Photomicrograph by Giulio Chiodi, in immersion; magnified 15×.

Consistent with the chemical formula of beryl ($Be_3Al_2Si_6O_{18}$), all the samples contained Si, Al, and Be as major elements. Minor but significant contents of Fe, Na, and Mg were recorded in the Canadian samples, whereas Na, Cs, and traces of K were recorded in the Maxixe-type sample. The Malossi synthetic blue beryls contained high amounts of Cu and Fe, as well as traces of Mg, Mn, and Na; however, Fe was the only minor element detected in the Tairus synthetic sample.

Figure 9. The average contents of Na_2O, MgO, MnO, FeO, CuO, and Cs_2O are shown for the various types of blue beryl investigated in the present study.

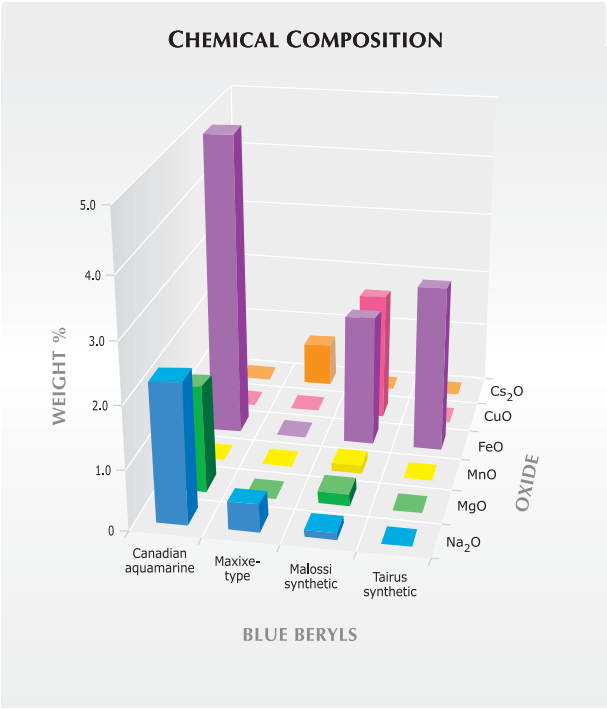

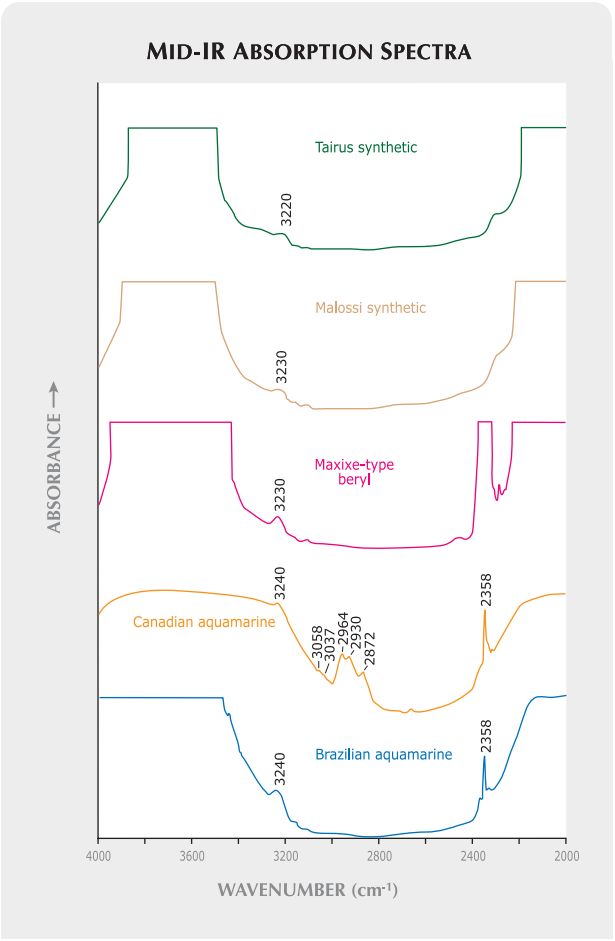

Figure 10. Representative mid-infrared spectra, taken in diffuse reflectance, showed features between 4000 and 3400 cm^{-1} (and to 3200 cm^{-1} in the Canadian material) related to their water contents. The CO_2-related signal at 2358 cm^{-1} in the aquamarines and Maxixe-type beryl have thus far never been found with this strength in synthetics. The peaks between 3000 and 2800 cm^{-1} in the Canadian aquamarine are related to the presence of a filler (for clarity enhancement).

Spectroscopy. Table 3 summarizes the most significant spectroscopic features of the natural, treated, and synthetic blue beryl samples we studied, which are described below.

Mid-Infrared. The mid-infrared spectra revealed a multitude of absorption bands (figure 10). For all the samples, two dominant areas of absorption saturated the detector in the 4000–3400 cm^{-1} (extending to 3200 cm^{-1} in the case of the Canadian aquamarines)

and 2250–400 cm^{-1} regions. A broad band centered between 3240 and 3220 cm^{-1} was also present in all samples. Another area of significant absorption was found at approximately 2400–2250 cm^{-1} (again, see figure 10). In addition, we observed a series of bands in the Canadian samples in the region between ~3000 and 2800 cm^{-1} (the most dominant were at 2964, 2930, and 2872 cm^{-1}).

The presence of water in the beryl structure may be determined by careful analysis of mid-IR spectra collected in transmission mode on powdered material in KBr pellets. This eliminates the total absorption that otherwise occurs in significant regions of that spectrum, although it does require some damage to the original specimen. The IR pattern of a Malossi synthetic beryl that we acquired by this

TABLE 3. Main spectroscopic features of the natural and synthetic blue beryls investigated in this study.

Spectral region	Natural			Synthetic	
	Aquamarine				
	Brazil	Canada		Malossi	Tairus
Mid-IR (4000–2000 cm^{-1})	Total absorption between 4000 and 3400 cm^{-1}, and a band at about 3240 cm^{-1}, related to water content	Total absorption between 4000 and 3200 cm^{-1}, with a band at 3240 cm^{-1}, related to water content (in transmission mode, resolved as 3591 and 3655 cm^{-1} due to type II H_2O) Peaks at 3058, 3037, 2964, 2930, and 2872 cm^{-1}, due to an artificial resin	Total absorption between 4000 and 3400 cm^{-1}, and a band at about 3230 cm^{-1}, related to water content	Total absorption between 4000 and 3400 cm^{-1}, and a band at 3230 cm^{-1}, related to water content (in transmission mode, resolved as 3595 and 3663 cm^{-1} due to type II H_2O, and 3698 cm^{-1} due to type I H_2O)	Total absorption between 4000 and 3400 cm^{-1}, and a band at about 3220 cm^{-1}, related to water content
	Sharp peak at about 2358 cm^{-1}, attributed to structural CO_2	Sharp peak at 2358 cm^{-1}, attributed to structural CO_2	Strong band at about 2358 cm^{-1}, attributed to structural CO_2		
Near-IR (9000–4000 cm^{-1})	Combination bands and overtones of types I and II water molecules	Combination bands and overtones of type II water molecules	Combination bands and overtones of types I and II water molecules	Combination bands and overtones of types I and II water molecules Total absorption between 9000 and 6500 cm^{-1}, likely due to the high Cu^{2+} content	Combination bands and overtones of types I and II water molecules
UV-Vis-NIR (250–850 nm)	Strong absorption band at 825 nm (o- and e-ray), due to Fe^{2+}; broad absorption band at about 640 nm (e-ray), assigned to a $Fe^{2+} \leftrightarrow Fe^{3+}$ charge process or to Fe^{2+} in the channels Peaks at 370 nm (o-ray) and 427 nm (e- and o-ray), associated with Fe^{3+}	Not tested	Set of bands over the 500–700 nm range (573, 588, 605, 625, 645, and 690 nm), related to a radiation-induced color center; also present were bands at 311 nm (e-ray) and 320 nm (o-ray)	Strong absorptions below 360 nm and beyond 580 nm (o-ray) and 610 nm (e-ray), due to a combination of Cu and Fe absorption features Peaks at 370 nm (o-ray) and 428 nm (e- and o-ray), associated with Fe^{3+} Bands at 475 and 540 nm (o-ray) and 568 nm (e-ray), probably due to Mn^{3+} (Ni^{3+} could contribute to the 475 nm absorption feature)	Strong absorption band at 825 nm (o- and e-ray), due to Fe^{2+}; broad absorption band at about 580 nm (e-ray), assigned to a $Fe^{2+} \leftrightarrow Fe^{3+}$ charge process or to Fe^{2+} in the channels Peaks at 370 nm (o-ray) and 428 nm (e- and o-ray) associated with Fe^{3+}

method revealed two dominant absorption bands at 3698 and 3595 cm^{-1}, with a weaker third band positioned at ~3663 cm^{-1}, while the Canadian aquamarine was characterized by two dominant bands at ~3655 and 3591 cm^{-1} (figure 11).

Near-Infrared. As illustrated in figure 12, the significant near-infrared absorption features—strong individual bands and a number of weaker bands—occurred in the regions of ~7300–6800 cm^{-1} and 5650–5000 cm^{-1}. Only the Malossi synthetic beryl exhibited total absorption beyond 6500 cm^{-1}.

UV-Vis-NIR. Polarized UV-Vis-NIR spectra in the 280–850 nm range for four samples are shown in figure 13. In general, all except the Maxixe-type blue beryl shared similar spectral features, characterized by a dominant absorption band at ~825 nm. In the spectra oriented perpendicular to the c-axis direction (e-ray), this band was modified by a side band at ~640 nm in the Brazilian aquamarine and ~580 nm in the Tairus synthetic samples. An additional band positioned at 427/428 nm was evident in spectra recorded for both the e-ray and o-ray, whereas a band at 370 nm was only present in spectra oriented along the o-ray, and a weak band at ~358 nm was recorded only along the e-ray.

In contrast, the absorptions recorded for the Maxixe-type sample consisted of a series of narrow

Figure 11. Alkali-rich Canadian aquamarine and low-alkali Malossi synthetic beryl show different mid-infrared absorption spectra taken in transmission mode on KBr pellets, because of different configurations of the water molecules hosted by the structural channels. Spectra offset vertically for clarity.

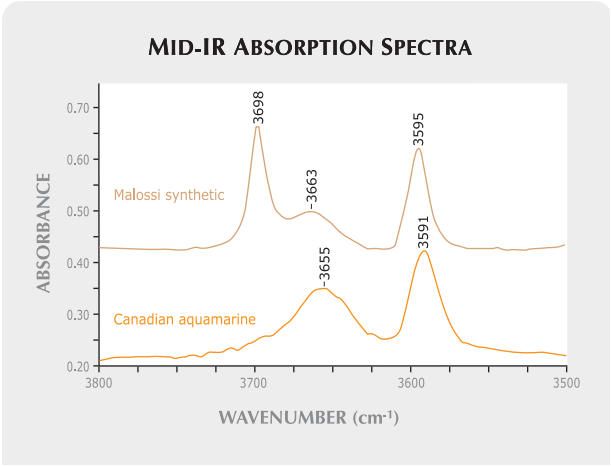

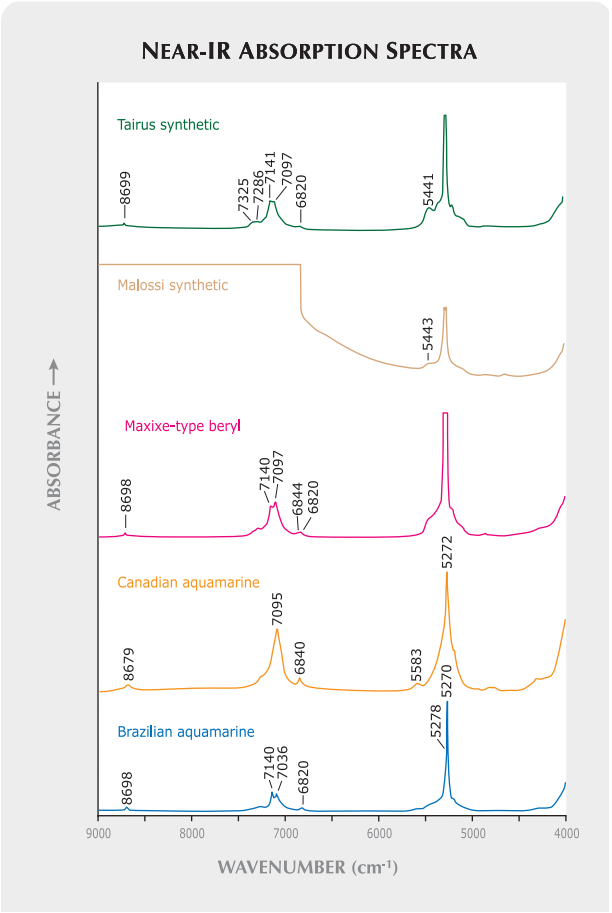

Figure 12. Near-infrared spectra in diffuse reflectance are shown for two aquamarines, a Maxixe-type beryl, and Malossi and Tairus synthetic blue beryls. All except the Canadian aquamarine (which is characterized by the absence of type I water molecules) exhibit somewhat similar combination bands and overtones of type I and II water molecules. Note that the Malossi sample exhibits total absorption between 9000 and 6500 cm^{-1}, most likely due to its high Cu^{2+} content.

bands between 500 and 700 nm, with the primary band positioned at ~690 nm, and a series of associated weaker bands at ~573, 588, 605, 625, and 645 nm (figure 13B). The stronger of this combined absorption was oriented along the c-axis direction (o-ray). Two additional, independent bands that also exhibited strongly pleochroic orientations were positioned at ~311 nm (e-ray) and 320 nm (o-ray).

The Malossi synthetic blue beryl was characterized by two strong absorptions, below about 360 nm and beyond ~580 nm (o-ray) and 610 nm (e-ray). A series of broad bands were also present, positioned at approximately 568 nm in the e-ray and at 475 and 540 nm in the o-ray orientations. The band at ~428 nm was evident in the spectra taken for both the

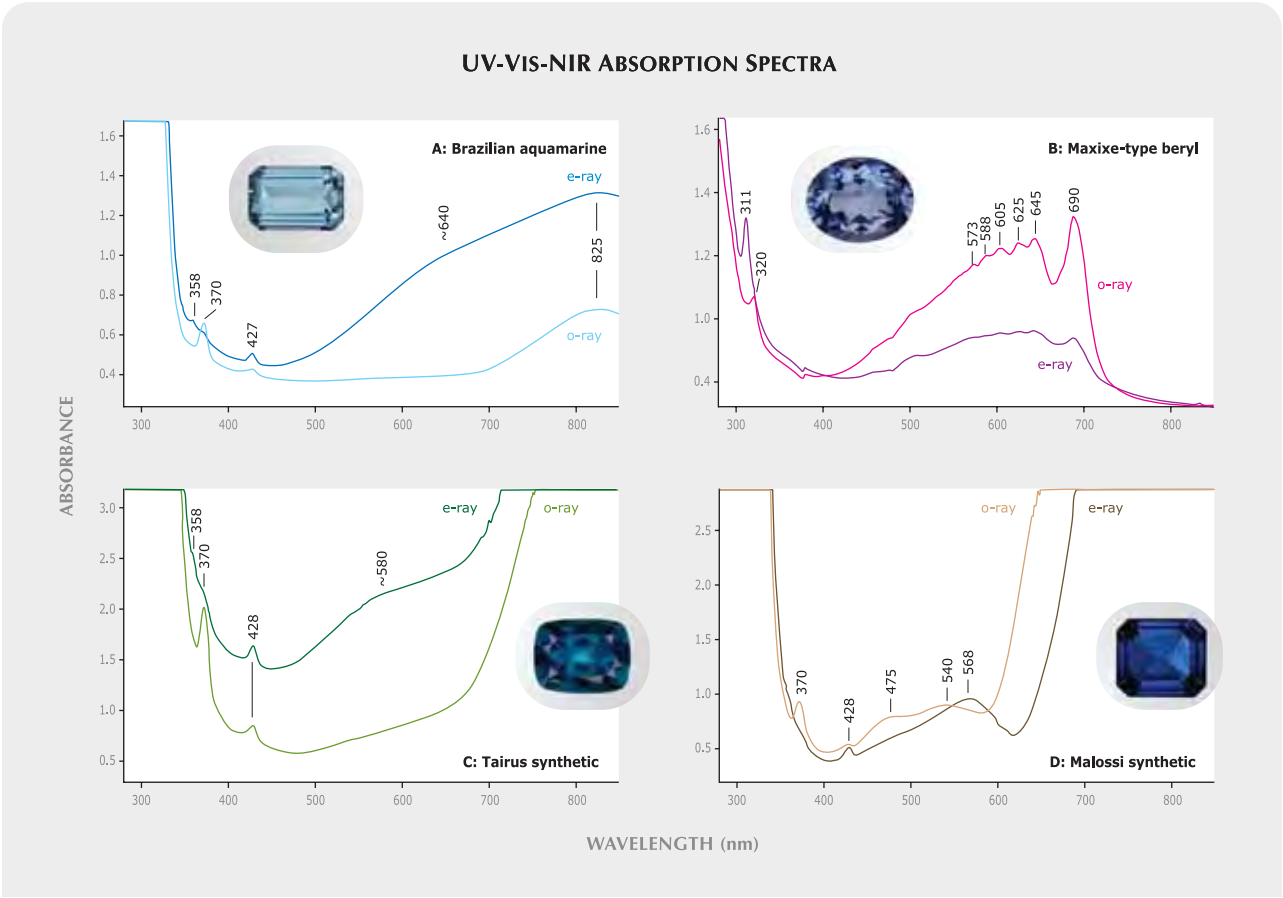

Figure 13. Polarized UV-Vis-NIR spectra are shown for four samples. The aquamarine and Tairus synthetic blue beryl exhibit absorption features associated with iron, whereas the pattern of the Malossi synthetic is mainly a combination of copper and iron absorptions. Manganese may be responsible for the broad bands at 475, 540, and 568 nm in the Malossi synthetic. The spectra of the Maxixe-type beryl are characterized by signals due to radiation-induced color centers.

e- and o-ray orientations, whereas the band at 370 nm was only present along the o-ray.

DISCUSSION

Standard Gemological Properties. The RI and SG values of the Brazilian and Nigerian samples were within the ranges reported for aquamarine (RI: 1.572–1.590; SG: 2.66–2.80; O'Donoghue, 2006). However, the Canadian samples had higher values, as previously reported by Rohtert et al. (2003). These differences are presumably related to the chemical composition (higher Fe, Mg, and Na) and denser inclusions of the Canadian beryls. The Maxixe-type (irradiated) sample had RI and SG values that are in agreement with the literature (e.g., Brown, 1993; Reinitz and Moses, 1997; Wentzell and Reinitz, 1997) and are virtually identical to those of natural Maxixe beryl (Brown, 1993). The RI and SG values of the Tairus synthetic specimens were similar to those reported by Schmetzer (1990) and Smirnov et al. (1999), whereas the Malossi synthetics had slightly higher values, owing to their compositional differences (notably, the presence of Cu). However, the overlap in the ranges of RI and SG values means that these properties cannot be used reliably to discriminate these materials from one another.

The anomalous dichroism of Maxixe-type, as well as Maxixe, beryls is a diagnostic marker (Brown, 1993; Nassau, 1996; Reinitz and Moses, 1997; Wentzell and Reinitz, 1998). As reported by Brown (1993), the green UV fluorescence shown by the Maxixe-type sample is indicative of irradiation treatment.

Microscopy. Magnification can provide important information for the separation of natural and synthetic blue beryl. Aquamarine and other natural blue beryls may be identified by a wide range of multi-

phase fluid inclusions; some mineral inclusions such as apatite, epidote, goethite, hematite, ilmenite, limonite, mica, quartz, spessartine, and tourmaline; as well as internal growth structures (see, e.g., Sinkankas, 1981; Lindt et al., 1986; Gübelin and Koivula, 2005).

All the synthetic blue beryls studied exhibited diagnostic internal features that proved their artificial nature and were distinctive of hydrothermal growth. These included strongly undulating, step- and chevron-like growth structures, which were similar to those that have been reported for hydrothermal synthetic emeralds (see, e.g., Schmetzer, 1988; Schmetzer et al., 1997; Sechos, 1997; Adamo et al., 2005; Gübelin and Koivula, 2005; Schmetzer et al., 2006). Residues of seed plates, when present, are also diagnostic of synthetic origin.

Chemical Composition. Our samples could be readily separated on the basis of their chemical composition. The Canadian aquamarines had the highest FeO contents ever reported in the literature for a blue gem beryl, which were consistent with values reported for Canadian blue beryl by other researchers (Rohtert et al., 2003; Turner et al., 2007). Aquamarine specimens from other localities (e.g., Brazil, Mozambique, Nigeria, Arizona, and Italy) are also characterized by the presence of iron (e.g., Schaller et al., 1962; Graziani and Di Giulio, 1979; Deer et al., 1986; Lind et al., 1986; Aurisicchio et al., 1988; Viana et al., 2002; Neiva and Neiva, 2005). Li, Na, Mg, K, Ca, and Cs are the most common minor elements usually present in aquamarine. Although the distinction of natural aquamarine from alkali-poor synthetic beryl was straightforward for most of the samples in our study, some natural stones—such as those from Nigeria (Lind et al., 1986)—have low alkali contents, so chemical composition alone should not be considered proof of origin. The absence of Fe, as well as of other chromophores, in irradiated Maxixe-type beryl and in untreated Maxixe beryl (Schlossmacher and Klang, 1935) will easily separate them from aquamarine.

The presence of copper (CuO average 2.07 wt.%) is diagnostic of Malossi synthetic beryl. This well-known chromophore produces an intense blue coloration in hydrothermal synthetic beryl (Koivula and Kammerling, 1988; Schmetzer et al., 2006). It is also present as a trace element in some hydrothermally grown synthetic emeralds (Schmetzer, 1988; Mashkovtsev and Smirnov, 2004; Adamo et al., 2005; Schmetzer et al., 2006). However, it has never been reported in any natural aquamarine, Maxixe-type beryl, or Maxixe beryl. For information on the position of Cu in the crystal structure of synthetic beryl, see Adamo et al. (2008).

Tairus synthetic blue beryl may be separated from alkali-rich natural aquamarines by its lower Fe content and absence of any significant Cu, Na, Mg, Mn, K, and Cs (see table 2 and Schmetzer et al., 2006). Again, though, for Na/Mg-poor natural aquamarines such as those from Nigeria (see, e.g., Lind et al., 1986), chemical composition alone does not provide a clear distinction.

Spectroscopy. *Mid-Infrared.* All the samples revealed total absorption in the region of ~2250–400 cm^{-1}, which is intrinsic to beryl, as well as ~4000–3400 cm^{-1}, which is related to the incorporation of water (see, e.g., Stockton, 1987; Adamo et al., 2005).

The strong 2358 cm^{-1} band found in natural aquamarines and Maxixe-type beryl is attributed to structural CO_2, which is commonly present in many natural and synthetic materials (Wood and Nassau, 1967, 1968; Stockton, 1987; Aines and Rossman, 1984; Charoy et al., 1996; Gatta et al., 2006; Andersson, 2006). In beryl, however, only the natural material can show a strong 2358 cm^{-1} peak; this feature is generally weak or absent in the synthetic beryl reported to date (Stockton, 1987; Koivula et al., 1996; Mashkovtsev and Smirnov, 2004; Choudhary and Golecha, 2007). We did not observe any of the characteristic bands attributed to chlorine and ammonium that are often found in hydrothermally grown synthetic emeralds (Schmetzer et al., 1997; Mashkovtsev and Solntsev, 2002; Mashkovtsev and Smirnov, 2004; Adamo et al., 2005).

The absorption features in the ~3000–2800 cm^{-1} range in the aquamarines from Canada indicate the presence of an organic, polymer-type filler (e.g., Johnson et al., 1999; Kiefert et al., 1999), in agreement with our microscopic observations.

The two dominant absorption bands at 3698 and 3595 cm^{-1} in the transmittance powder FTIR spectrum of the Malossi synthetic blue beryl indicate the occurrence of water molecules in two different configurations [type I and type II (Wood and Nassau, 1967, 1968; Schmetzer and Kiefert, 1990; Charoy et al., 1996; Mashkovtsev and Smirnov, 2004)]. The third, weaker and structured absorption band at approximately 3663 cm^{-1} is usually also associated with type II H_2O (Wood and Nassau, 1967, 1968; Farmer, 1974; Aines and Rossman, 1984; Charoy et al., 1996; Viana et al., 2002; Mashkovtsev and Smirnov, 2004),

BOX A: IDENTIFICATION

SEPARATION BETWEEN NATURAL AND SYNTHETIC BLUE BERYL

We found that the Malossi and Tairus synthetic blue beryls could be separated from their natural counterparts on the basis of the following characteristics:

Microscopic Features. The strongly irregular and distinctive growth pattern we observed in all the synthetic samples provides clear evidence of hydrothermal synthesis. When present, the tiny black inclusions and seed-plate residues seen in the Tairus synthetic beryls are also diagnostic of hydrothermal growth in a laboratory. Natural blue beryl may be identified by a wide range of multi-phase fluid inclusions, various mineral inclusions, as well as internal growth structures.

Chemical Composition. All aquamarines are characterized by the presence of iron, which acts as the primary chromophore. Li, Na, Mg, K, Ca, and Cs also can be present in variable amounts. In the case of high and moderate alkali-bearing aquamarines, separation from the alkali-poor Tairus synthetics is possible, but this fails in the case of some Na/Mg-poor aquamarines, such as Nigerian material. The presence of copper (average 2.07 wt.% CuO) in Malossi synthetic blue beryl allows a rapid distinction from natural beryl.

Spectroscopic Measurements. Infrared spectroscopy can be diagnostic if one is able to establish the type of water molecules: If type I H_2O is absent, the beryl specimen may be classified as natural; otherwise, the IR pattern is not distinctive. The detection of Cu by Vis-NIR is typical of the Malossi material.

SEPARATION OF AQUAMARINE FROM MAXIXE AND MAXIXE-TYPE BERYL

We believe the following features provide means to distinguish between aquamarine and Maxixe/Maxixe-type beryl:

Optical Properties: Dichroism. Both Maxixe and Maxixe-type beryls show pleochroic behavior with the dominant blue color parallel to the c-axis (i.e., down the o-ray), which is the opposite of natural aquamarine and the hydrothermally grown synthetics.

Other Gemological Properties. Most Maxixe/Maxixe-type beryls fade on exposure to light and/or heat. A green UV fluorescence reaction, when present, provides an additional indicator that the material is Maxixe-type beryl.

Chemical Composition. The Fe chromophore is absent in Maxixe and Maxixe-type beryls, but it is abundant in all aquamarine from various localities. This confirms that the cause of color in Maxixe and Maxixe-type beryl is a radiation-induced color center.

Spectroscopic Measurements. In keeping with their chemistry, no evidence of iron-related features occurs in the UV-Vis-NIR spectra of Maxixe and Maxixe-type beryls. A visible spectrum with a series of bands positioned between 500 and 700 nm will readily identify them. Color centers associated with the different impurities in Maxixe and Maxixe-type beryls result in slightly different UV-Vis-NIR spectra for these two materials.

although it may also be related to hydroxyl ions (Schmetzer and Kiefert, 1990; Aurisicchio et al., 1994) and/or to a third type of water molecule (Andersson, 2006). Such a combination of type I and II water in beryl is typical of low-alkali-content synthetic and natural beryl (Schmetzer and Kiefert, 1990). In contrast, the IR spectrum of the Canadian aquamarine is distinctive in its absence of the 3698 cm^{-1} absorption feature (type I H_2O), and it is generally diagnostic of an alkali-rich beryl (Schmetzer and Kiefert, 1990).

Near-Infrared. The near-infrared spectra (9000–4000 cm^{-1}) of all our samples revealed several absorption features that can be attributed to combination bands and overtones of water molecules incorporated into the beryl structure. These spectral features are related to the presence of both type I and II water molecules (Wood and Nassau, 1967; Mashkovtsev and Smirnov, 2004), except for the Canadian aquamarine, which has no features related to type I H_2O, as highlighted by mid-IR spectroscopy in transmission mode. The occurrence of total absorption beyond ~6500 cm^{-1}, attributable to the presence of Cu^{2+} (Mashkovtsev and Smirnov, 2004; Adamo et al., 2005; Schmetzer et al., 2006), is typical of the Malossi synthetic material.

UV-Vis-NIR. The Brazilian aquamarines and the Tairus synthetic blue beryls revealed a typical aquamarine spectrum, with a dominant absorption band positioned at ~825 nm (with polarization both parallel and perpendicular to the o-ray) due to Fe^{2+} on two different lattice positions (Wood and Nassau, 1968; Goldman et al., 1978; Schmetzer, 1990; Burns, 1993; Taran and Rossman, 2001; Viana et al., 2002). A side band positioned at ~640 nm in the natural aquamarine and ~580 nm in the Tairus synthetic material (with polarization perpendicular to the o-ray) is also present. This absorption feature has been assigned by some to an $Fe^{2+} \leftrightarrow Fe^{3+}$ charge-transfer process (e.g., Goldman et al., 1978; Schmetzer, 1990; Burns, 1993; Taran and Rossman, 2001), whereas others (e.g., Wood and Nassau, 1968; Viana et al., 2002) have suggested that it arises from Fe^{2+} in the structural channels. The peaks at 370 and 428 nm are related to Fe^{3+} (Goldman et al., 1978; Schmetzer, 1990; Burns, 1993; Viana et al., 2002; Adamo et al., 2005).

Distinctive of the Malossi synthetic blue beryl was a very strong absorption (even more intense than in other samples) starting at ~610 nm (e-ray) and 580 nm (o-ray) and extending to 1500 nm in the near-IR region, which may result from a combination of copper and iron absorptions (see, e.g., Mashkovtsev and Smirnov, 2004; Adamo et al., 2005; Schmetzer et al., 2006). The 370 and 428 nm Fe^{3+} absorption features were also present. The broad bands centered at 475, 540, and 568 nm are probably related to Mn^{3+}, a chromophore known to produce pink, red, and violet hues in beryl (Burns, 1993; Shigley et al., 2001). Ni^{3+} might also contribute to the broad absorption feature at about 475 nm (o-ray; Schmetzer, 1990), in agreement with its presence among the trace elements measured by LA-ICP-MS in one Malossi sample (see data in Adamo et al., 2008).

The presence in the Maxixe-type beryl of narrow absorption features in the 500–700 nm range, with the dominant band at ~690 nm, as well as the vibronic structure that extends toward 400 nm, has been attributed to color centers associated with carbonate impurities that have been activated by irradiation (Nassau et al., 1976; Edgar and Vance, 1977; Andersson, 1979; Nassau and Prescott, 1981; Nassau, 1996; Mathew et al., 1998; Andersson, 2006). In the original Maxixe beryl, these color centers are associated instead with nitrate impurities, causing a slightly different visible spectrum (Andersson, 1979, Nassau, 1996). Thus, the UV-Vis-NIR spectra for both Maxixe and Maxixe-type beryls provide reliable means to distinguish these gem materials from aquamarine.

CONCLUSIONS

Aquamarine, Maxixe-type beryl, and hydrothermally grown synthetic blue beryl may be readily distinguished using a combination of gemological, chemical, and spectroscopic features (see box A). Careful observation of pleochroism, fluorescence, and internal features (with magnification) can provide useful indicators for gemologists with basic equipment. More-sophisticated techniques such as UV-Vis-NIR and mid-infrared spectroscopy, as well as chemical analysis, can provide clear proof of the identification.

ABOUT THE AUTHORS

Dr. Adamo (ilaria.adamo@unimi.it) is a postdoctoral fellow, Dr. Pavese is professor of mineralogy, and Dr. Gatta is a researcher in the Earth Sciences Department of the University of Milan, Italy. Dr. Prosperi is director of the Italian Gemological Institute (IGI) laboratory, Milan. Dr. Diella is a senior researcher of the Environmental Processes Dynamics Institute (IDPA), National Research Council (CNR), Section of Milan, to which Dr. Pavese and Dr. Gatta also belong. Dr. Ajò is director of the Inorganic and Surface Chemistry Institute (ICIS), National Research Council (CNR), Padua, Italy, and is responsible for the CNR coordination group for Gemological Materials Research. Mr. Smith is vice president and chief gemologist at American Gemological Laboratories (AGL) in New York City.

ACKNOWLEDGMENTS

The authors would like to thank Greg Davison (True North Gems, Vancouver, Canada) for providing the blue beryl specimens from the True Blue property in the Yukon Territory, Canada; the Italian Gemological Institute for providing aquamarine samples from Brazil, the Maxixe-type blue beryl specimen, and the Tairus hydrothermal synthetic blue beryls; Alberto Malossi (Malossi Gemme Create, Milan) for providing the Malossi synthetic blue beryl samples; and C. R. "Cap" Beesley (AGL) for providing the aquamarine samples from Brazil and Nigeria. Dr. Giulio Chiodi (Vicenza, Italy), Fred Kahn, and Sun Joo Chung (AGL) are gratefully acknowledged for some photos. The authors are indebted for technical assistance to: Dr. Vanda Rolandi (University of Milan—Bicocca, Italy) and Stefano Villa (IGI, Milan) for collaboration in the collection of photomicrographs; Dr. Marcello Picollo, Bruno Radicati (CNR, Florence), and Franco De Zuane (CNR, Padua) for preliminary nonpolarized UV-Vis-NIR spectroscopy; and Dr. Nicola Rotiroti (University of Milan) for collaboration in X-ray single-crystal data collection and structure refinement. Dr. Karl Schmetzer (Petershausen, Germany) is thanked for his useful suggestions. The manuscript benefited considerably from the critical reviews of Dr. Lee A. Groat and Dr. Michael S. Krzemnicki. This study was supported through the Ingenio Global Grant project by the European Social Fund, the Italian Ministry of Labour and Welfare, and the Lombardy Region.

REFERENCES

Adamo I., Gatta G.D., Rotiroti N., Diella V., Pavese A. (2008) Gemmological investigation of a synthetic blue beryl: A multi-methodological study. *Mineralogical Magazine* (in press).

Adamo I., Pavese A., Prosperi L., Diella V., Merlini M., Gemmi M., Ajò D. (2005) Characterization of the new Malossi hydrothermal synthetic emerald. *Gems & Gemology*, Vol. 41, No. 4, pp. 328–338.

Aines R.D., Rossman G.R. (1984) The high temperature behavior of water and carbon dioxide in cordierite and beryl. *American Mineralogist*, Vol. 69, No. 3/4, pp. 319–327.

Andersson L.O. (1979) The difference between Maxixe beryl and Maxixe-type beryl: An electron paramagnetic resonance investigation. *Journal of Gemmology*, Vol. 16, No. 5, pp. 313–317.

Andersson L.O. (2006) The position of H^+, Li^+ and Na^+ impurities in beryl. *Physics and Chemistry of Minerals*, Vol. 33, No. 6, pp. 403–416.

Aurisicchio C., Fioravanti G., Grubessi O., Zanazzi P.F. (1988) Reappraisal of the crystal chemistry of beryl. *American Mineralogist*, Vol. 73, No. 7/8, pp. 826–837.

Aurisicchio C., Grubessi O., Zecchini P. (1994) Infrared spectroscopy and crystal chemistry of the beryl group. *Canadian Mineralogist*, Vol. 32, No. 1, pp. 55–68.

Brown G. (1993) Maxixe-type beryls. Ghost from the past. *Australian Gemmologist*, Vol. 18, No. 7, pp. 215–221.

Burns R.G. (1993) *Mineralogical Applications of Crystal Field Theory*, 2nd ed. Cambridge Topics in Mineral Physics and Chemistry, Cambridge University Press, Cambridge, UK.

Charoy B., De Donato P., Barres O., Pinto-Coelho C. (1996) Channel occupancy in an alkali-poor beryl from Serra Branca (Goiás, Brazil): Spectroscopic characterization. *American Mineralogist*, Vol. 81, No. 3/4, pp. 395–403.

Choudhary G., Golecha C. (2007) Gem News International: New Tairus synthetic beryl simulating "Paraíba" tourmaline. *Gems & Gemology*, Vol. 43, No. 4, pp. 385–387.

Deer W.A., Howie R.A., Zussman J. (1986) *Disilicates and Ring Silicates. Rock-Forming Minerals*, Vol. 1B, Geological Society of London, UK, pp. 373–409.

Edgar A., Vance E.R. (1977) Electron paramagnetic resonance, optical absorption, and magnetic circular dichroism studies of the CO_3^- molecular-ion in irradiated natural beryl. *Physics and Chemistry of Minerals*, Vol. 1, No. 2, pp. 165–178.

Farmer V.C. (1974) *The Infrared Spectra of Minerals*. Mineralogical Society, London.

Gatta G.D., Nestola F., Bromiley G.D., Mattauch S. (2006) The real topological configuration of the extra-framework content in alkali-poor beryl: A multi-methodological study. *American Mineralogist*, Vol. 91, No. 1, pp. 29–34.

Goldman D.S., Rossman G.R., Parkin K.M. (1978) Channel constituents in beryl. *Physics and Chemistry of Minerals*, Vol. 3, No. 3, pp. 225–235.

Graziani G., Di Giulio V. (1979) Growth of aquamarine crystal from Brazil. *Neues Jahrbuch für Mineralogie—Monatshefte*, Vol. 3, pp. 101–108.

Gübelin E.J., Koivula J.I. (2005) *Photoatlas of Inclusions in Gemstones*, Vol. 2. Opinio Publishers, Basel, Switzerland.

Johnson M.L., Elen S., Muhlmeister S. (1999) On the identification of various emerald filling substances. *Gems & Gemology*, Vol. 35, No. 2, pp. 82–107.

Kiefert L., Hänni H.A., Chalain J-P., Weber W. (1999) Identification of filler substances in emeralds by infrared and Raman spectroscopy. *Journal of Gemmology*, Vol. 26, No. 8, pp. 501–520.

Koivula J.I., Kammerling R.C. (1988) Gem News: Unusual synthetic beryls from the Soviet Union. *Gems & Gemology*, Vol. 24, No. 4, pp. 252–253.

Koivula J.I., Kammerling R.C. (1991) Gem News: More Soviet synthetics. *Gems & Gemology*, Vol. 27, No. 1, pp. 55.

Koivula J.I., Kammerling R.C., DeGhionno D., Reinitz I., Fritsch E., Johnson M.L. (1996) Gemological investigation of a new type of Russian hydrothermal synthetic emerald. *Gems & Gemology*, Vol. 32, No. 1, pp. 32–39.

Laurs B.M. (2005) Gem News International: Saturated blue aquamarine from Nigeria. *Gems & Gemology*, Vol. 41, No. 1, p. 56.

Lind T., Schmetzer K., Bank H. (1986) Blue and green beryls (aquamarines and emeralds) of gem quality from Nigeria. *Journal of Gemmology*, Vol. 20, No. 1, pp. 40–48.

Mashkovtsev R.I., Smirnov S.Z. (2004) The nature of channel constituents in hydrothermal synthetic emerald. *Journal of Gemmology*, Vol. 29, No. 3, pp. 129–141.

Mashkovtsev R.I., Solntsev V.P. (2002) Channel constituents in synthetic beryl: Ammonium. *Physics and Chemistry of Minerals*, Vol. 29, No. 1, pp. 65–71.

Mathew G., Karanthy R.V., Gundu Rao T.K., Deshpande R.S. (1998) Maxixe-type colour centre in natural colourless beryl from Orissa, India: An ESR and OA investigation. *Journal of Gemmology*, Vol. 26, No. 4, pp. 238–251.

Nassau K. (1990) Synthetic gem materials in the 1980s. *Gems & Gemology*, Vol. 26, No. 1, pp. 50–63.

Nassau K. (1996) On the identification and fade testing of Maxixe beryl, golden beryl and green aquamarine. *Journal of Gemmology*, Vol. 25, No. 2, pp. 108–115.

Nassau K. (1997) The chronology of synthetic gemstones. *Journal of Gemmology*, Vol. 25, No. 7, pp. 453–516.

Nassau K., Prescott B.E. (1981) Nonfading Maxixe-type beryl? *Gems & Gemology*, Vol. 17, No. 4, pp. 217–219.

Nassau K., Prescott B.E., Wood D.L. (1976) The deep blue Maxixe-type color center in beryl. *American Mineralogist*, Vol. 61, No. 1/2, pp. 100–107.

Neiva A.M.R., Neiva M.C.J. (2005) Beryl from the granitic pegmatite at Nativo, Alto Ligonha, Mozambique. *Neues Jahrbuch für Mineralogie, Abhandlungen*, Vol. 181, No. 2, pp. 173–182.

O'Donoghue M. (2006) *Gems*, 6th ed. Butterworth-Heinemann, Oxford, UK.

Reinitz I., Moses T. (1997) Lab Notes: Beryl, treated color. *Gems & Gemology*, Vol. 33, No. 4, p. 293.

Roebling W., Tromnau H.W. (1935) Maxixeberyll. II. *Zentralblatt für Mineralogie, Geologie und Paläontologie*, Vol. A, pp. 134–139.

Rohtert W.R., Quinn E.P., Groat L.A., Rossman G.R. (2003) Gem News International: Blue beryl discovery in Canada. *Gems & Gemology*, Vol. 39, No. 4, pp. 327–329.

Schaller W.T., Stevens R.E., Jahns R.H. (1962) An unusual beryl from Arizona. *American Mineralogist*, Vol. 47, No. 5/6, pp. 672–699.

Schlossmacher K., Klang H. (1935) Der Maxixeberyll. I. *Zentralblatt für Mineralogie, Geologie und Paläontologie*, Vol. A, pp. 37–44.

Schmetzer K. (1988) Characterization of Russian hydrothermally grown synthetic emeralds. *Journal of Gemmology*, Vol. 21, No. 3, pp. 145–164.

Schmetzer K. (1990) Hydrothermally grown synthetic aquamarine manufactured in Novosibirsk, USSR. *Gems & Gemology*, Vol. 26, No. 3, pp. 206–211.

Schmetzer K., Kiefert L. (1990) Water in beryl—A contribution to the separability of natural and synthetic emeralds by infrared spectroscopy. *Journal of Gemmology*, Vol. 22, No. 4, pp. 215–223.

Schmetzer K., Kiefert L., Bernhardt H-J., Beili Z. (1997) Characterization of Chinese hydrothermal synthetic emerald. *Gems & Gemology*, Vol. 33, No.4, pp. 276–291.

Schmetzer K., Schwarz D., Bernhardt H-J, Häger T. (2006) A new type of Tairus hydrothermally-grown synthetic emerald, coloured by vanadium and copper. *Journal of Gemmology*, Vol. 30, No. 1/2, pp. 59–74.

Sechos B. (1997) Identifying characteristics of hydrothermal synthetics. *Australian Gemmologist*, Vol. 19, No. 9, pp. 383–388.

Shigley J.E., McClure S.F., Cole J.E., Koivula J.I., Lu T., Elen S., Demianets L.N. (2001) Hydrothermal synthetic red beryl from the Institute of Crystallography, Moscow. *Gems & Gemology*, Vol. 37, No. 1, pp. 42–55.

Sinkankas J. (1981) *Emerald and Other Beryls*. Chilton Book Co., Radnor, PA.

Smirnov S., Mashkovtsev R., Thomas V., Maltsev V., Alexey I., Anastasiya B. (1999) New hydrothermal synthetic gemstones from Tairus, Novosibirsk, Russia. *Gems & Gemology*, Vol. 35, No. 3, pp. 175–176.

Stockton C.M. (1987) The separation of natural from synthetic emerald. *Gems & Gemology*, Vol. 23, No. 2, pp. 96–99.

Taran M.N., Rossman G.R. (2001) Optical spectroscopy study of tuhualite and a re-examination of the beryl, cordierite, and osumilite spectra. *American Mineralogist*, Vol. 86, No. 9, pp. 973–980.

Turner D., Groat L.A., Hart C.J.R., Mortensen J.K., Linnen R.L., Giuliani G., Wengzynowski W. (2007) Mineralogical and geochemical study of the True blue aquamarine showing, southern Yukon. *Canadian Mineralogist*, Vol. 45, No. 2, pp. 203–227.

Viana R.R., Jordt-Evangelista H., Magela da Costa G., Stern W.B. (2002) Characterization of beryl (aquamarine variety) from pegmatites of Minas Gerais, Brazil. *Physics and Chemistry of Minerals*, Vol. 29, No. 10, pp. 668–679.

Wentzell C.Y., Reinitz I. (1998) Lab Notes: Maxixe beryl, faded and fading. *Gems & Gemology*, Vol. 34, No. 4, pp. 284–285.

Wood D.L., Nassau K. (1967) Infrared spectra of foreign molecules in beryl. *Journal of Chemical Physics*, Vol. 47, No. 7, pp. 2220–2228.

Wood D.L., Nassau K. (1968) The characterization of beryl and emerald by visible and infrared absorption spectroscopy. *American Mineralogist*, Vol. 53, No. 5/6, pp. 777–800.